Analysis, Modeling, and Validation for the Thermal Dynamics of a Polymer Electrolyte Membrane Fuel Cell System

Eric A. Müller
Measurement and Control Laboratory,
ETH Zentrum,
8092 Zurich, Switzerland
e-mail: mueller@imrt.mavt.ethz.ch

Anna G. Stefanopoulou
Fuel Cell Control Systems Laboratory,
The University of Michigan,
Ann Arbor, MI 48109
e-mail: annastef@umich.edu

A control-oriented mathematical model of a polymer electrolyte membrane (PEM) fuel cell stack is developed and experimentally verified. The model predicts the bulk fuel cell transient temperature and voltage as a function of the current drawn and the inlet coolant conditions. The model enables thermal control synthesis and optimization and can be used for estimating the transient system performance. Unlike other existing thermal models, it includes the gas supply system, which is assumed to be capable of controlling perfectly the air and hydrogen flows. The fuel cell voltage is calculated quasistatically. Measurement data of a 1.25 kW*, 24-cell fuel cell stack with an integrated membrane-type humidification section is used to identify the system parameters and to validate the performance of the simulation model. The predicted thermal response is verified during typical variations in load, coolant flow, and coolant temperature. A first-law control volume analysis is performed to separate the relevant from the negligible contributions to the thermal dynamics and to determine the sensitivity of the energy balance to sensor errors and system parameter deviations.* [DOI: 10.1115/1.2173663]

Keywords: PEM fuel cell system, thermal dynamics, control volume analysis, first-law analysis, energy balance, sensitivity analysis, mathematical modeling, lumped-parameter approach, control-oriented model

Introduction

Fuel cells (FCs) are considered as an alternative power source for automotive propulsion, electricity generation, and back-up power supplies. As the heat they generate in the range of power needed for a typical passenger vehicle or for a residential power supply cannot be passively dissipated, and as virtually all applications have demanding transient requirements, thermal management is necessary. Besides maintaining the fuel cell temperature within a relatively narrow range, warming up the system in a fast and energy-efficient manner is a particularly critical task for every type of fuel cell application. Hence, to ensure optimal system performance, an accurate and robust controller for thermal management is vitally important, even for low-temperature fuel cells such as the polymer electrolyte membrane (PEM) fuel cells.

In order to systematically develop controllers for the thermal management, to on-line optimize the warm-up phase, or to simulate the transient behavior of a fuel cell system, a control-oriented model of the system's thermal dynamics is required. Moreover, a profound knowledge of the flows and their contributions to the energy and mass balance is imperative to model the system efficiently.

Several modeling approaches of various levels of complexity have been proposed recently. Important results can be found in Refs. [1–4]. Amphlett et al. [1] have proposed a simple dynamic model for a PEM fuel cell stack which, given a set of gas feed and operating conditions, predicts fuel cell voltage and stack temperature as a function of time. Lee and Lalk in [2] developed a technique for modeling fuel cell stacks. Since models developed using this technique are intended to be used to investigate different operating and design configurations, they are relatively complex. The work of Xue et al. [3] established a transient model of a PEM fuel cell system which includes manifold and capacitance dynamic effects. Parts of the model are correlated to a single-cell experimental investigation. Zhang et al. [4] presented a simple model of an entire PEM fuel cell stack thermal system, including coolant loop and radiator, in which the stack thermal dynamic behavior is reduced to a single state considering only two energy flows, namely, the heat generated by the reaction and the heat transferred to the cooling medium.

Those models are not ideally suited for control and real-time estimation purposes. Either they are too complex and thus are computationally demanding, require a lot of effort to be parametrized, or they have not been tested through variations in coolant flow, temperature, and stack power. In addition, none of the papers cited provides a quantitative analysis of the various effects influencing the fuel cell thermal dynamics.

The objectives of this study are to first analyze and prioritize energy flows in PEM fuel cell systems with respect to their contributions to the thermal balance. Then, a control-oriented mathematical model of the fuel cell system thermal dynamics that can be used for the model-based design of temperature controllers, to optimize the warm-up phase of the system, or which can be implemented as an extension of a static fuel cell system model is derived. The model must predict the system temperature and the stack voltage as a function of just the coolant inlet conditions and the electrical current demand. It must capture the relevant static and dynamic effects without being computationally demanding, and has to be easy to parametrize.

To this end, this paper first describes the 1.25 kW, 24-cell fuel cell system investigated and the experimental setup that allows us to perform control experiments for the parametrization and the model validation. A first-law control volume analysis is per-

Manuscript received March 17, 2005; final manuscript received September 14, 2005. Review conducted by Abel Hernandez.

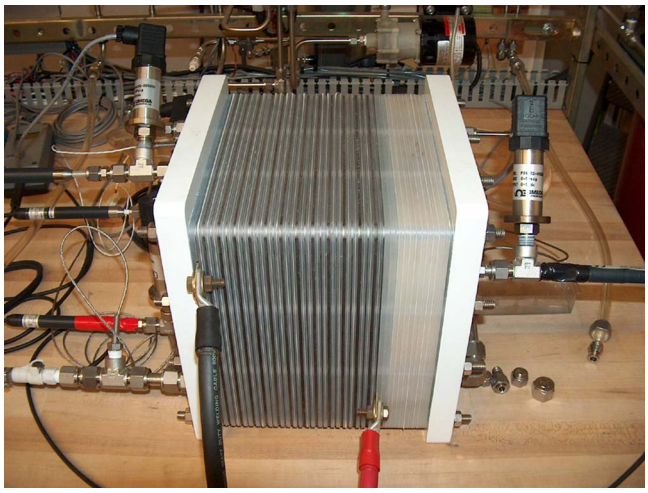

Fig. 1 Test bench of a 1.25 kW, 24-cell fuel cell stack with an integrated membrane-type humidification section

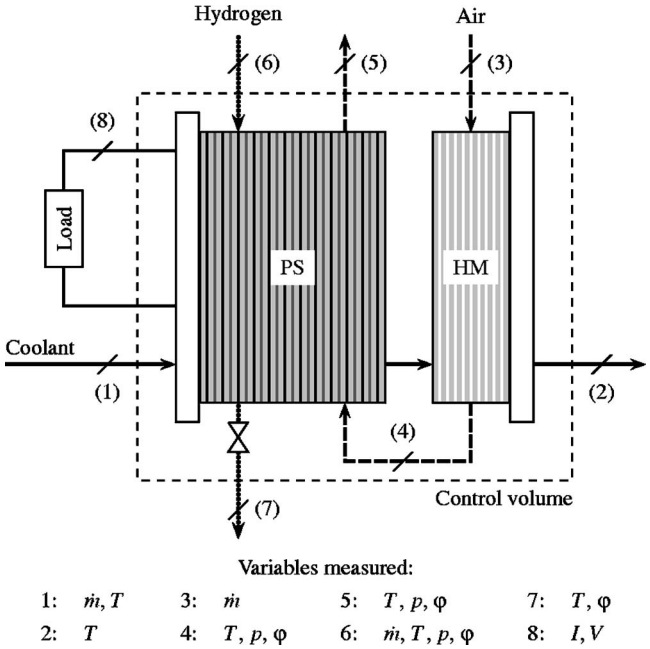

Fig. 2 Schematic diagram of the fuel cell stack with integrated humidification section and measurement locations (1–8)

formed, verified, and discussed. For a set of experimental data recorded on the test bench, an energy and a water mass balance are evaluated. A differentiation is made of relevant and negligible contributions to the thermal dynamics. The control volume analysis also forms the basis for a sensitivity analysis which rates the impact of sensor errors or parameter uncertainties on the energy balance. Based on these investigations, the structure of a control-oriented, lumped-parameter mathematical model is proposed. The model includes the gas supply system and accounts for the heat generated by the electrochemical reaction, the vapor and product water flow enthalpies on the cathode side (including humidification), the surface heat losses, and the heat transferred to the deionized water of the coolant circuit. An existing static electrochemical model is used to calculate the fuel cell voltage. The gas supply system is assumed to be statically and perfectly controlled, which is a reasonable assumption due to the large bandwidth separation between the gas supply system and the thermal system. Where necessary, parameter values are identified with measurement data recorded on the test bench. Finally, the model is implemented and its prediction is validated with two different sets of experimental data.

Fuel Cell System Investigated

Figure 1 shows the instrumented stack installed on the test station at the University of Michigan's Fuel Cell Control Laboratory. The stack has 24 PEM fuel cells with GORE™ PRIMEA® series 56 membrane electrode assemblies (MEAs). The stack was designed and assembled at the Schatz Energy Research Center at Humboldt State University. Its MEAs have 0.4 mg/cm^2 and 0.6 mg/cm^2 platinum loading on the anode and cathode, respectively. The catalyst support is carbon black. To diffuse gas from the flow fields to the membrane, double-sided, hydrophobic, version 3 Etek™ ELATs® were used. The flow fields are comprised of machined graphite plates. The stack contains an internal humidification section that diffuses water vapor after the power section coolant loop to the incoming air through a GORE™ SELECT® membrane. There are two fuel cells per cooling plate in the power section. The stack can produce 1.25 kW continuous power at less than 600 mA/cm^2. It is designed for operation at low temperatures ($<70°C$), and at low gauge pressures (<12 kPa in the cathode and 14–34 kPa in the anode).

Experimental Setup. Protruding from the stack endplates in Fig. 1 are the transducers for relative humidity, temperature, and pressure. Their location is also shown in the schematic diagram of Fig. 2. The inlet coolant flow rate (location 1 in Fig. 2) is measured with a McMillan 101-8 Flo-Sensor with a range of 0–5 slm[1] and an accuracy of ±0.02 slm. Two resistance temperature devices with a range of −40°C to 85°C and an accuracy of ±0.3°C measure the coolant temperatures at the inlet of the power section and at the outlet of the humidification section (locations 1 and 2 in Fig. 2). An MKS type 1559A air flow controller (co-located sensor) with a range of 20–200 slm, an accuracy of ±2 slm, and a response time of 0.5 s is installed upstream of the air inlet (location 3 in Fig. 2). A Hastings HFM201 hydrogen mass flow meter with a range of 0–100 slm, ±1 slm, and a response time of 2 s is installed upstream of the anode inlet (location 6 in Fig. 2). Four relative humidity (RH) sensors are installed in the inlets and outlets of the cathode and anode manifolds within the stack (locations 4–7 in Fig. 2). The RH sensors are capacitive-based Rotronic SP05 probes with an integrated transmitter and a resistance temperature device. The RH sensor range is 0–100% with an accuracy of ±1.5%. Three Omega PX4202-005G5V pressure transducers with a range of 0–5 psig, an accuracy of ±0.012 psig, and a response time of 10 ms are used at locations 4–6 in Fig. 2. The current drawn from the stack is controlled and measured by a Dynaload RBL488 electronic load with a range of 0–500 A (±0.015 A). Individual cell voltages are measured with 0–1200 mV/cell (±1 mV/cell) and added together to calculate the stack voltage. The sensor specifications were provided by the manufacturers and have not been independently verified. The data acquisition system is based on PCI DAQ boards with signal conditioning 5B backplane hardware and LabVIEW™ software. Data logging occurs at 2 Hz.

The fuel cell operates on a test station with integrated controls, diagnostics, and safety mechanisms. The air control system regulates the air flow at a desired stoichiometric level (200–400%) or at a fixed air flow value. The MKS air flow controller handles dry air supplied by an Atlas-Copco SF1-4 stationary oil-free air scroll-type compressor though an integrated dryer and pressure-controlled ballast tank. The fuel is stored in high-pressure, high-purity hydrogen cylinders. The hydrogen control system reduces

[1]Standard liters per minute (slm) are the units used by the manufacturer. Although SI units are used in the rest of this article, the instrument specifications are quoted with the manufacturer's units.

the pressure to a level appropriate for delivery to the fuel cell stack and then regulates the anode pressure to a desired level, which is typically set higher than the cathode pressure. Deionized water is used as a cooling medium in the test station to either heat or cool the stack using electric resistance heating and a heat exchanger with a controllable (on-off) fan. The thermostatic controller accepts a set-point and upper-lower thresholds for the power section outlet temperature of the coolant. An electric pump recirculates the coolant through a reservoir that is refilled when a low value is reached due to evaporation. The coolant flow rate is controlled through a manual valve.

Control Volume Analysis

The control volume considered includes both the fuel cell stack power section (PS) and the humidification section (HM), as indicated in Fig. 2. There are six mass streams crossing the boundary of the control volume: the coolant, the air, and the hydrogen flows entering and leaving the system. The dissipation of electric power is accounted for outside of the control volume.

Energy Balance. An energy balance is performed to ensure that all the relevant flows in the stack are considered and to verify the measurement and sensor calibrations. The energy balance is further used to assess the importance of each contribution and the sensitivity of certain assumptions and the accuracy of the measurements.

In order to do a first-law control volume analysis, all contributions to the energy balance have to be determined. The summation of energy flows due to mass flows into and out of the control volume, the net rate of heat transfer, and the net rate of work are included. For the control volume sketched in Fig. 2, the first law of thermodynamics can be represented by the following differential equation:

$$\frac{dU}{dt} = \dot{H}_{\mathrm{Reac}} - \dot{H}_{\mathrm{H_2O}}^{\mathrm{Evap\ PS}} + \Delta\dot{H}_{\mathrm{Gases}}^{\mathrm{nonReac}} + \Delta\dot{H}_{\mathrm{Ct}} - \dot{H}_{\mathrm{H_2O}}^{\mathrm{Evap\ HM}} - \dot{Q}_{\mathrm{Conv}}^{\mathrm{B2Amb}} - \dot{Q}_{\mathrm{Rad}}^{\mathrm{B2Amb}} - P_{\mathrm{El}} \tag{1}$$

This equation states that the rate of change of energy inside the control volume, dU/dt, is equal to the reaction enthalpy rate (for liquid product water), minus the evaporation enthalpy flow rate of water inside the power section, plus the individual enthalpy flow rate differences of the nonreacting parts of the gas streams, plus the enthalpy flow rate difference of the coolant, minus the evaporation enthalpy flow rate of the diffused coolant (humidification), minus the rate of heat transfer to the environment, minus the electric power. Kinetic and potential energies of the mass streams can be neglected, as they are small compared to the other contributions. Mass storage effects are not considered, either. A detailed discussion of the relevant contributions to the energy balance follows.

The reaction of hydrogen and oxygen to form liquid water is an exothermic chemical reaction. The energy flow rate of this reaction is calculated as the difference between the enthalpy flow rates of formation of the reactants (hydrogen and oxygen) and the enthalpy flow rate of formation of the product (liquid water) at the inlet and outlet, respectively,

$$\dot{H}_{\mathrm{Reac}} = \dot{m}_{\mathrm{H_2}}^{\mathrm{Reac}}(h_f^0 + \Delta h)_{\mathrm{H_2}} + \dot{m}_{\mathrm{O_2}}^{\mathrm{Reac}}(h_f^0 + \Delta h)_{\mathrm{O_2}} - \dot{m}_{\mathrm{H_2O}}^{\mathrm{Reac}}(h_f^0 + \Delta h)_{\mathrm{H_2O}(l)} \tag{2}$$

where $\dot{m}$ denotes the mass flow rates of the substances, h_f^0 the mass specific enthalpies of formation with respect to a reference state, and Δh the mass specific enthalpy differences from the present state to the reference state. The mass flow rates of the reactants and the product are calculated from the measured electric current as

$$\dot{m}_{\mathrm{H_2}}^{\mathrm{Reac}} = M_{\mathrm{H_2}} n_{\mathrm{Cells}} \frac{1}{2F} I_{\mathrm{St}} \tag{3}$$

$$\dot{m}_{\mathrm{O_2}}^{\mathrm{Reac}} = M_{\mathrm{O_2}} n_{\mathrm{Cells}} \frac{1}{4F} I_{\mathrm{St}} \tag{4}$$

$$\dot{m}_{\mathrm{H_2O}}^{\mathrm{Reac}} = M_{\mathrm{H_2O}} n_{\mathrm{Cells}} \frac{1}{2F} I_{\mathrm{St}} \tag{5}$$

where M denotes the molecular weights in kg/mol, n_{Cells} is the number of fuel cells in the stack, and F is the Faraday constant. Constant specific heats are assumed for the enthalpy changes with respect to the reference state of the substances,

$$\Delta h_{\mathrm{H_2}} = C_{p0\ \mathrm{H_2}}(T_{\mathrm{mH_2}}^{\mathrm{PS\ In}} - T_0) \tag{6}$$

$$\Delta h_{\mathrm{O_2}} = C_{p0\ \mathrm{O_2}}(T_{\mathrm{mAir}}^{\mathrm{HM\ In}} - T_0) \tag{7}$$

$$\Delta h_{\mathrm{H_2O}(l)} = C_{p\ \mathrm{H_2O}(l)}(T_{\mathrm{mAir}}^{\mathrm{PS\ Out}} - T_0) \tag{8}$$

where T_0 is the reference temperature. The air temperature at the humidifier inlet, $T_{\mathrm{mAir}}^{\mathrm{HM\ In}}$, is not measured in our experimental setup (location 3 in Fig. 2), and it is, thus, considered as constant. Its value is later shown to affect weakly the energy balance. As indicated in Eq. (8), the liquid product water is assumed to exit on the cathode side.

In order to determine the contribution of the electrochemical reaction, the product water is assumed to be in liquid form. A change in the state of aggregation of water is coupled to a change in enthalpy: the evaporation of water removes energy from the system, whereas the condensation of vapor releases energy. By determining the difference of water vapor entering and leaving the power section, the enthalpy flow rate due to evaporation (or condensation) can be calculated,

$$\begin{aligned}\dot{H}_{\mathrm{H_2O}}^{\mathrm{Evap\ PS}} = {} & (\dot{m}_{\mathrm{H_2O}}^{\mathrm{mAir\ PS\ Out}} - \dot{m}_{\mathrm{H_2O}}^{\mathrm{mAir\ PS\ In}}) \cdot h_{fg\ \mathrm{H_2O}}(T_{\mathrm{mAir}}^{\mathrm{PS\ Out}}) \\ & + (\dot{m}_{\mathrm{H_2O}}^{\mathrm{mH_2\ PS\ Out}} - \dot{m}_{\mathrm{H_2O}}^{\mathrm{mH_2\ PS\ In}}) \cdot [h_{fg\ \mathrm{H_2O}}(T_{\mathrm{mH_2}}^{\mathrm{PS\ Out}}) \\ & - C_{p\ \mathrm{H_2O}(l)}(T_{\mathrm{mAir}}^{\mathrm{PS\ Out}} - T_{\mathrm{mH_2}}^{\mathrm{PS\ Out}})]\end{aligned} \tag{9}$$

The specific evaporation enthalpies, h_{fg}, are functions of the respective temperatures. As the liquid product water is assumed to exit on the cathode side, an enthalpy difference between cathode and anode has to be considered in Eq. (9) for the part of the product water exhausted on the anode side. The mass flow rates of water vapor at the cathode inlet and outlet (locations 4 and 5 in Fig. 2) can be calculated from the temperature, pressure, and relative humidity values, as follows:

$$\dot{m}_{\mathrm{H_2O}}^{\mathrm{mAir\ PS\ In}} = \frac{M_{\mathrm{H_2O}}}{M_{\mathrm{Air}}} \dot{m}_{\mathrm{Air}}^{\mathrm{HM\ In}} \cdot \frac{\varphi_{\mathrm{mAir}}^{\mathrm{PS\ In}} p_{\mathrm{Sat\ H_2O}}(T_{\mathrm{mAir}}^{\mathrm{PS\ In}})}{p_{\mathrm{mAir}}^{\mathrm{PS\ In}} - \varphi_{\mathrm{mAir}}^{\mathrm{PS\ In}} p_{\mathrm{Sat\ H_2O}}(T_{\mathrm{mAir}}^{\mathrm{PS\ In}})} \tag{10}$$

$$\dot{m}_{\mathrm{H_2O}}^{\mathrm{mAir\ PS\ Out}} = \frac{M_{\mathrm{H_2O}}}{M_{\mathrm{Air}}} \dot{m}_{\mathrm{Air}}^{\mathrm{Excess}} \cdot \frac{\varphi_{\mathrm{mAir}}^{\mathrm{PS\ Out}} p_{\mathrm{Sat\ H_2O}}(T_{\mathrm{mAir}}^{\mathrm{PS\ Out}})}{p_{\mathrm{mAir}}^{\mathrm{PS\ Out}} - \varphi_{\mathrm{mAir}}^{\mathrm{PS\ Out}} p_{\mathrm{Sat\ H_2O}}(T_{\mathrm{mAir}}^{\mathrm{PS\ Out}})} \tag{11}$$

where in Eq. (11), M_{Air} is used to approximate the molecular weight of the excess air. The mass flow rate of dry air entering the system, $\dot{m}_{\mathrm{Air}}^{\mathrm{HM\ In}}$, is measured (location 3 in Fig. 2). The mass flow rate of excess air is calculated as the inlet mass flow rate minus the mass flow rate of oxygen consumed by the reaction,

$$\dot{m}_{\mathrm{Air}}^{\mathrm{Excess}} = \dot{m}_{\mathrm{Air}}^{\mathrm{HM\ In}} - \dot{m}_{\mathrm{O_2}}^{\mathrm{Reac}} \tag{12}$$

Similarly, at the anode inlet and outlet (locations 6 and 7 in Fig. 2) the mass flow rates of water vapor can be determined as

$$\dot{m}_{H_2O}^{mH_2\ PS\ In} = \frac{M_{H_2O}}{M_{H_2}} \dot{m}_{H_2}^{PS\ In} \cdot \frac{\varphi_{mH_2}^{PS\ In} p_{Sat\ H_2O}(T_{mH_2}^{PS\ In})}{p_{mH_2}^{PS\ In} - \varphi_{mH_2}^{PS\ In} p_{Sat\ H_2O}(T_{mH_2}^{PS\ In})} \tag{13}$$

$$\dot{m}_{H_2O}^{mH_2\ PS\ Out} = \frac{M_{H_2O}}{M_{H_2}} \dot{m}_{H_2}^{Purge} \cdot \frac{\varphi_{mH_2}^{PS\ Out} p_{Sat\ H_2O}(T_{mH_2}^{PS\ Out})}{p_{mH_2}^{PS\ Out} - \varphi_{mH_2}^{PS\ Out} p_{Sat\ H_2O}(T_{mH_2}^{PS\ Out})} \tag{14}$$

The pressure at the anode outlet, $p_{mH_2}^{PS\ Out}$, is not measured but can be safely approximated as the ambient pressure. The inlet hydrogen flow, $\dot{m}_{H_2}^{PS\ In}$, is measured. The mass flow rate of purged hydrogen is calculated as the inlet mass flow rate of hydrogen, minus the mass flow rate consumed by the reaction, minus the hydrogen lost by leakage,

$$\dot{m}_{H_2}^{Purge} = \dot{m}_{H_2}^{PS\ In} - \dot{m}_{H_2}^{Reac} - \dot{m}_{H_2}^{Leak} \tag{15}$$

where the mass flow rate of leaking hydrogen, $\dot{m}_{H_2}^{Leak}$, is estimated during a few operating points without purge flow (dead-ended anode).

The reaction enthalpy term, $\dot{H}_{Reac}$, covers the enthalpies of the reactant mass flows of the electrochemical reaction. However, these mass flows differ from the mass flows entering the system on the cathode as well as on the anode side. Specifically, the oxygen participating in the reaction is only one part of the moist air entering the system and a certain amount of hydrogen is typically used for purging the anode or is lost through leakage. The enthalpy contributions of these gas mixtures which are only passing through the system, therefore, have to be calculated separately,

$$\Delta\dot{H}_{Gases}^{nonReac} = \Delta\dot{H}_{mAir}^{Excess} + \Delta\dot{H}_{mH_2}^{Purge} + \Delta\dot{H}_{H_2}^{Leak} \tag{16}$$

In order to determine the enthalpy flow rates of the moist air, excluding the reacting oxygen, and of the purged moist hydrogen, the Dalton model is used. Hence, it is assumed that the enthalpy of a gas mixture can be evaluated as the sum of the enthalpies of the components,

$$\Delta\dot{H}_{mAir}^{Excess} = \Delta\dot{H}_{Air}^{Excess} + \Delta\dot{H}_{H_2O}^{Excess} \tag{17}$$

$$\Delta\dot{H}_{mH_2}^{Purge} = \Delta\dot{H}_{H_2}^{Purge} + \Delta\dot{H}_{H_2O}^{Purge} \tag{18}$$

For the calculation of the enthalpies, again, perfect gas behavior (constant specific heats) is assumed,

$$\Delta\dot{H}_{Air}^{Excess} = \dot{m}_{Air}^{Excess} C_{p0\ Air} (T_{mAir}^{HM\ In} - T_{mAir}^{PS\ Out}) \tag{19}$$

$$\Delta\dot{H}_{H_2O}^{Excess} = \dot{m}_{H_2O}^{mAir\ HM\ In} C_{p0\ H_2O(g)} (T_{mAir}^{HM\ In} - T_{mAir}^{PS\ Out}) \tag{20}$$

and

$$\Delta\dot{H}_{H_2}^{Purge} = \dot{m}_{H_2}^{Purge} C_{p0\ H_2} (T_{mH_2}^{PS\ In} - T_{mH_2}^{PS\ Out}) \tag{21}$$

$$\Delta\dot{H}_{H_2O}^{Purge} = \dot{m}_{H_2O}^{mH_2\ PS\ In} C_{p0\ H_2O(g)} (T_{mH_2}^{PS\ In} - T_{mH_2}^{PS\ Out}) \tag{22}$$

The specific heat of air is used to approximate the specific heat of the excess air from which the reactant oxygen was removed. Note that a possible change of the state of aggregation of the water carried by the moist air and the moist hydrogen is accounted for in Eq. (9). As defined above (Eq. (13)), the mass flow rate of water vapor at the anode inlet, $\dot{m}_{H_2O}^{mH_2\ PS\ In}$, can be calculated from the temperature, pressure, and relative humidity values. On the air side, the mass flow rate of water vapor entering the humidification section, $\dot{m}_{H_2O}^{mAir\ HM\ In}$, is assumed to be negligible. This assumption is reasonable because the air flows through a dryer before it enters the mass air flow controller and the humidification section. Moreover, this assumption does not affect significantly the energy balance as shown later. A certain amount of hydrogen is always lost through leakage (not marked in the schematic of Fig. 2). The enthalpy flow rate associated with the hydrogen leak is

$$\Delta\dot{H}_{H_2}^{Leak} = \dot{m}_{H_2}^{Leak} C_{p0\ H_2} [T_{mH_2}^{PS\ In} - \tfrac{1}{2}(T_{mH_2}^{PS\ In} + T_{mH_2}^{PS\ Out})] \tag{23}$$

The temperature at which the leakage occurs is assumed to be the mean of the anode inlet and outlet temperatures.

Now, the energy contribution from the coolant is explained. The coolant enters the system at the power section inlet (location 1 in Fig. 2), partially evaporates into the air stream inside the humidification section, and exits the system as liquid fraction into the coolant loop at the humidifier outlet (location 2 in Fig. 2) and as vapor fraction at the cathode outlet (location 5 in Fig. 2). Hence, the respective contribution of the liquid part to the energy balance is the enthalpy flow rate of the coolant at the power section inlet minus the enthalpy flow rate of the coolant at the humidifier outlet,

$$\Delta\dot{H}_{Ct} = \dot{m}_{Ct}^{PS\ In} C_{p\ H_2O(l)} (T_{Ct}^{PS\ In} - T_{Ct}^{HM\ Out}) \tag{24}$$

The enthalpy flow rate of the evaporated part of the coolant is calculated as

$$\dot{H}_{H_2O}^{Evap\ HM} = \dot{m}_{H_2O}^{Evap\ HM} [h_{fg\ H_2O}(T_{Ct}^{HM\ Out}) - C_{p0\ H_2O(g)} (T_{Ct}^{HM\ Out} - T_{mAir}^{PS\ Out})] \tag{25}$$

It is assumed that the coolant evaporates at the temperature $T_{Ct}^{HM\ Out}$. The water contents of the air stream at the humidifier inlet (location 3 in Fig. 2) and of the air stream at the humidifier outlet (location 4 in Fig. 2) are used to calculate the mass flow rate of coolant evaporated,

$$\dot{m}_{H_2O}^{Evap\ HM} = \dot{m}_{H_2O}^{mAir\ HM\ Out} - \dot{m}_{H_2O}^{mAir\ HM\ In} \tag{26}$$

At the humidifier inlet, as mentioned above, the water mass flow rate is assumed to be equal to zero. The water mass flow rate at the humidifier outlet is equivalent to the water mass flow rate at the power section inlet (Eq. (10)),

$$\dot{m}_{H_2O}^{mAir\ HM\ Out} = \dot{m}_{H_2O}^{mAir\ PS\ In} \tag{27}$$

As the temperatures of the fuel cell system body and its surroundings differ, heat is lost through the body's surface. The heat transfer to the surrounding area consists of a convective and a radiative heat flow,

$$\dot{Q}_{Conv}^{B2Amb} = (\alpha A)_{B2Amb} (T_{Syst} - T_{Amb}) \tag{28}$$

$$\dot{Q}_{Rad}^{B2Amb} = \varepsilon\sigma A_{B2Amb} (T_{Syst}^4 - T_{Amb}^4) \tag{29}$$

The convective heat transfer coefficient, α_{B2Amb}, is a function of the medium properties, the ambient air flow, and the geometry. The coefficient was determined using standard heat transfer correlations for natural convection [5]. As the coefficient differs for horizontal and vertical surfaces, the surface area was partitioned, and the coefficients for the vertical area elements, the horizontal upper, and the horizontal lower areas were calculated separately. The overall heat transfer coefficient was then calculated as the area-weighted sum of the individual coefficients. A rough estimation is used for the emissivity of the body, ε. The parameter A_{B2Amb} denotes the outer surface area of the body, σ is the Stefan-Boltzmann constant, T_{Amb} represents the temperature of the environment, and T_{Syst} is the system temperature.

Depending on the amount of current drawn and other influencing quantities (e.g., system temperature), the fuel cell stack produces an output voltage. The electric power delivered by the system equals the product of this stack voltage, V_{St}, and the current drawn, I_{St},

$$P_{El} = V_{St} I_{St} \tag{30}$$

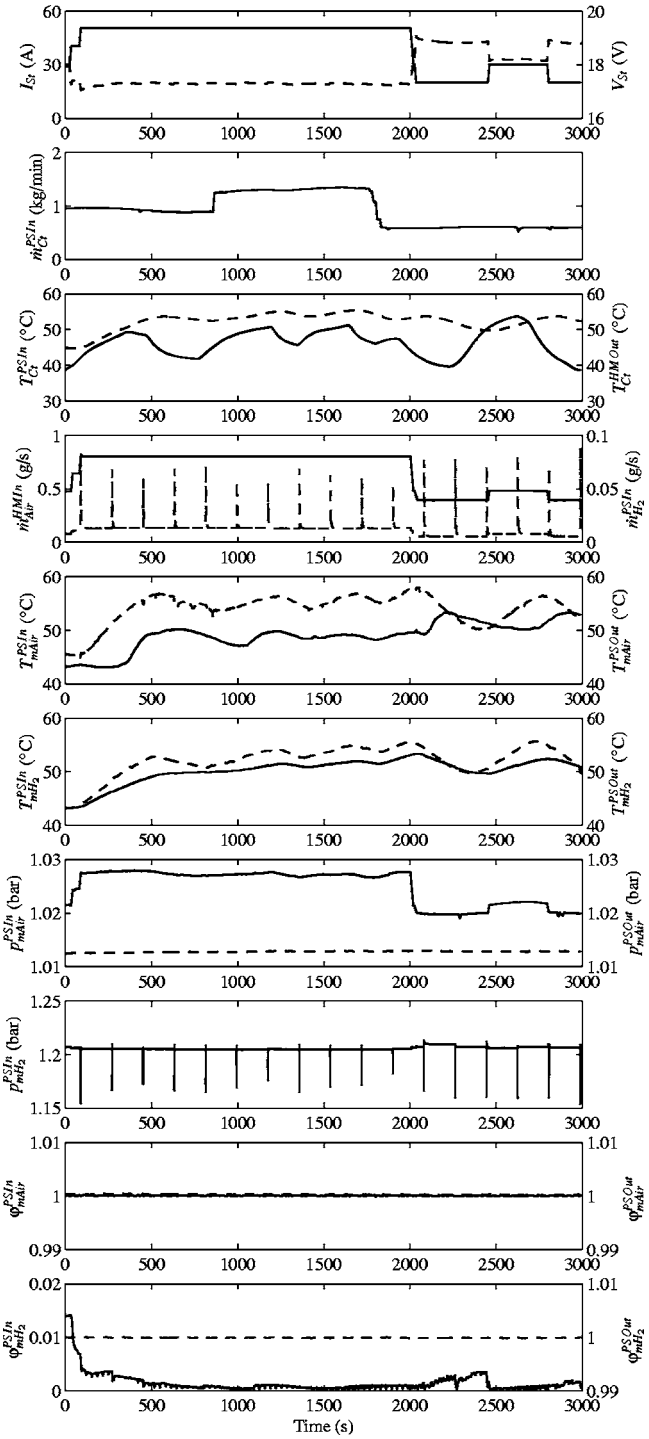

Fig. 3 Experimental data used for evaluation of the control volume analysis and for model parameter identification; left axes: solid lines, right axes: dashed lines

Experimental Results for Energy Balance

The energy balance is evaluated with a set of measurement data acquired on the test bench. The measurement data result from an experimental run during which the fuel cell system was operated at different power levels and with different coolant inlet conditions. In Fig. 3 all sensor data are plotted against time. In the first subplot, the electric current and the resulting stack voltage are shown. The electric power drawn from the system changes between about 350 W and 900 W. The second subplot shows the coolant mass flow rate. The coolant mass flow rate varies between 0.6 kg/min and 1.4 kg/min. The coolant inlet temperature, which is a function of the heat exchanger fan operation, fluctuates within the range of about 40°C to 55°C. The coolant inlet and outlet temperatures are depicted in subplot three. Subplot four shows the controlled air and hydrogen mass flow rates. The remaining six subplots show the properties of the air and the hydrogen at power section inlet and outlet, respectively. These are the temperatures, pressures, and relative humidities. Note that the pressure at the anode outlet is not measured. There are no measurements of the temperature and of the humidity of the air stream at the humidifier inlet, nor of the mass flow rate of leaking hydrogen, either. These nonmeasured quantities are estimated as follows:

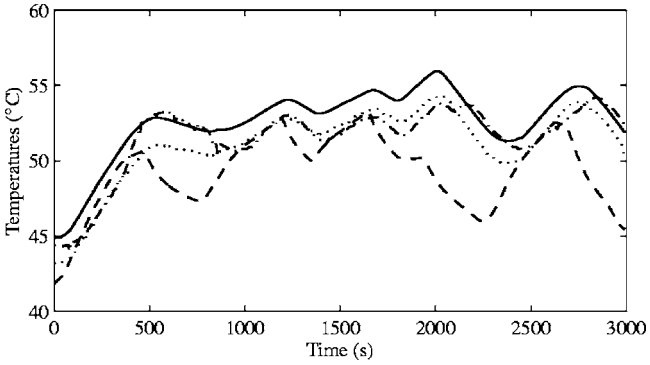

Fig. 4 Comparison of temperature curves; calculated system temperature (—), coolant temperature (– – –), cathode temperature (–·), and anode temperature (···)

- $T_{\mathrm{mAir}}^{\mathrm{HM\ In}}=20\,^{\circ}\mathrm{C}$
- $\dot{m}_{\mathrm{H_2O}}^{\mathrm{mAir\ HM\ In}}=0$ mg/s
- $p_{\mathrm{mH_2}}^{\mathrm{PS\ Out}}=1.013$ bar
- $\dot{m}_{\mathrm{H_2}}^{\mathrm{Leak}}=0.56$ mg/s.

The ambient temperature was set constant to

- $T_{\mathrm{Amb}}=25\,^{\circ}\mathrm{C}$.

The effects of these values to the energy balance are analyzed later.

If all the measurement data, together with the estimations of the nonmeasured quantities stated above, are inserted into Eq. (2) to Eq. (30) and eventually into Eq. (1), a nonlinear differential equation results,

$$m_{\mathrm{Syst}}C_{\mathrm{Syst}}\frac{dT_{\mathrm{Syst}}}{dt}=f(T_{\mathrm{Syst}},t) \tag{31}$$

where $m_{\mathrm{Syst}}C_{\mathrm{Syst}}$ is the thermal capacity of the system. By integrating this differential equation, the temperature of the fuel cell system, T_{Syst}, can be calculated as a function of time. As no measurement of the system temperature exists the calculated system temperature is compared with the available temperature data to verify the control volume analysis. In Fig. 4 the calculated system temperature curve is plotted, together with the coolant temperature, the cathode temperature and the anode temperature. The latter three are presumed to be the means of the measured system input and output temperatures of the respective mass streams. The system temperature was initialized with the coolant outlet temperature. Clearly, the calculated system temperature is close to the other temperatures and exhibits reasonable transient behavior. Since Eq. (31) is an open integrator except for the influence of the heat losses to the ambient, small deviations in the energy balance would result in a divergence of the calculated system temperature. The general agreement of the measured and cal-

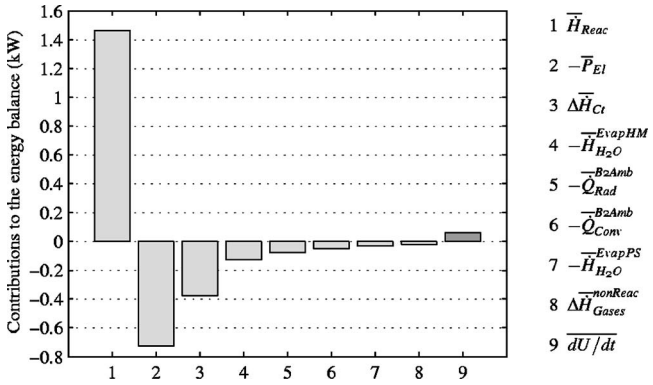

Fig. 5 Averaged contributions to the energy balance of the fuel cell system for the experimental run shown in Fig. 3

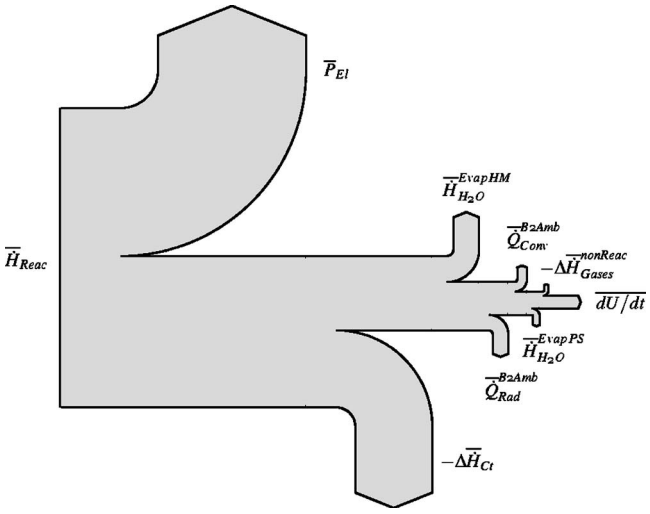

Fig. 6 Fuel cell system energy flow chart for the experimental run shown in Fig. 3

culated temperatures indicates that the experimental setup is free of significant measuring errors, that the assumptions in the control volume analysis are admissible, and that the values of the nonmeasured quantities and of the system parameters are reasonable. A detailed sensitivity analysis is provided in a subsequent section.

The energy balance reveals the influence of the different energy flows on the thermal dynamics of the system. In order to gain detailed insights, it is useful to analyze the individual contributions to the change in internal energy of the fuel cell system. Therefore, for the measurement data of Fig. 3 every term of Eq. (1) is calculated separately. To facilitate the comparison, all contributions are averaged over the duration of the experiment (indicated with a bar $\overline{(\,)}$). These mean contributions to the change in internal energy of the fuel cell system are depicted in a bar graph (Fig. 5) and listed in Table 1 as absolute values as well as in comparison to the average energy flow associated with the electrochemical reaction. In order to further clarify the flows, Fig. 6 shows the results in a flow chart. For the experiment investigated, the average energy flow contributed by the electrochemical reaction ($\dot{H}_{\mathrm{Reac}}$) is 1460 W. About half of it (726 W) is usable electric power (P_{El}), the remainder is waste heat. The main part (51%) of the waste heat is carried away by the coolant loop ($\Delta\dot{H}_{\mathrm{Ct}}$), another 17% as latent heat of the evaporated coolant ($\dot{H}_{\mathrm{H_2O}}^{\mathrm{Evap\ HM}}$). The heat losses to the environment ($\dot{Q}_{\mathrm{Rad}}^{B2\mathrm{Amb}}$, $\dot{Q}_{\mathrm{Conv}}^{B2\mathrm{Amb}}$) amount to 17% of the total waste heat, whereas both the radiative and the convective losses are of a similar magnitude. A fraction of 7.0% of the waste heat is used to evaporate product water ($\dot{H}_{\mathrm{H_2O}}^{\mathrm{EvapP\ S}}$) and heat up the nonreacting gases ($\Delta\dot{H}_{\mathrm{Gases}}^{\mathrm{nonReac}}$). The remaining waste heat (8.4%) is used to heat up the system (dU/dt). By far the smallest contributions to the energy balance stem from the hydrogen leakage and the purging. Despite the higher specific heat of hydrogen, the enthalpy difference of the purged moist hydrogen is between two and three orders of magnitude smaller than that of the moist excess air. This is mainly caused by the significant difference in the mass flow rates of anode and cathode flows and the smaller temperature change between inlet and outlet of the anode flow.

Table 1 Averaged energy flows of the fuel cell system for the experimental data shown in Fig. 3

Term	Absolute value (W)	Fraction of $\overline{\dot{H}}_{\mathrm{Reac}}$ (%)
$\overline{dU/dt}$	62.1	4.2
$\overline{\dot{H}}_{\mathrm{Reac}}$	1460	100
$\overline{\dot{H}}_{\mathrm{H_2O}}^{\mathrm{EvapP\ S}}$	31.7	2.2
$\Delta\overline{\dot{H}}_{\mathrm{mAir}}^{\mathrm{Excess}}$	20.3	1.4
$\Delta\overline{\dot{H}}_{\mathrm{mH_2}}^{\mathrm{Purge}}$	0.0233	0.0016
$\Delta\overline{\dot{H}}_{\mathrm{H_2}}^{\mathrm{Leak}}$	0.00760	0.00052
$\Delta\overline{\dot{H}}_{\mathrm{Ct}}$	376	26
$\overline{\dot{H}}_{\mathrm{H_2O}}^{\mathrm{Evap\ HM}}$	126	8.6
$\overline{\dot{Q}}_{\mathrm{Conv}}^{B2\mathrm{Amb}}$	47.4	3.2
$\overline{\dot{Q}}_{\mathrm{Rad}}^{B2\mathrm{Amb}}$	75.6	5.2
$\overline{P}_{\mathrm{El}}$	726	50

Water Mass Balance. A water mass balance for the gas channels inside the power section is developed similarly to the energy balance presented above. If no storage of water inside the system is assumed, the water mass balance is represented by the following equation:

$$0 = \dot{m}_{\mathrm{H_2O}}^{\mathrm{Reac}} + \dot{m}_{\mathrm{H_2O}}^{\mathrm{mAir\ PS\ In}} + \dot{m}_{\mathrm{H_2O}}^{\mathrm{mH_2\ PS\ In}} - \dot{m}_{\mathrm{H_2O}}^{\mathrm{mAir\ PS\ Out}} - \dot{m}_{\mathrm{H_2O}}^{\mathrm{mH_2\ PS\ Out}} - \dot{m}_{\mathrm{H_2O}}^{\mathrm{Liq\ Out}} \tag{32}$$

stating that the mass flow rate of water produced within the system plus the mass flow rate of water entering the system equals the mass flow rate of outgoing water, where the mass flow rate of water flowing into the cathode is equivalent to the mass flow rate of water exiting the humidification section,

$$\dot{m}_{\mathrm{H_2O}}^{\mathrm{mAir\ PS\ In}} = \dot{m}_{\mathrm{H_2O}}^{\mathrm{Evap\ HM}} + \dot{m}_{\mathrm{H_2O}}^{\mathrm{mAir\ HM\ In}} \tag{33}$$

The first five mass flow rates of Eq. (32) can be calculated as defined in the energy balance section (Eqs. (5), (10), (13), (11), and (14)). The mass flow rate of water exiting the gas channels in liquid form, $\dot{m}_{\mathrm{H_2O}}^{\mathrm{Liq\ Out}}$, is then determined from the mass balance (Eq. (32)).

Experimental Results for Water Mass Balance. The contributions to the water mass balance of Eq. (32) are calculated for the experimental data shown in Fig. 3 and averaged over the duration of the experiment (indicated with a bar $\overline{(\,)}$). In Fig. 7 the average (steady-state) water mass balance is shown in a flow chart, and the individual averaged mass flow rates are depicted in a bar graph. The amount of water produced by the electrochemical reaction is proportional to the electric current. For the electric output power of 726 W a water mass flow rate of approximately 93 mg/s is produced ($\dot{m}_{\mathrm{H_2O}}^{\mathrm{Reac}}$). The product water exits the system as liquid and also as vapor, as it is partially evaporated inside the fuel cells. In

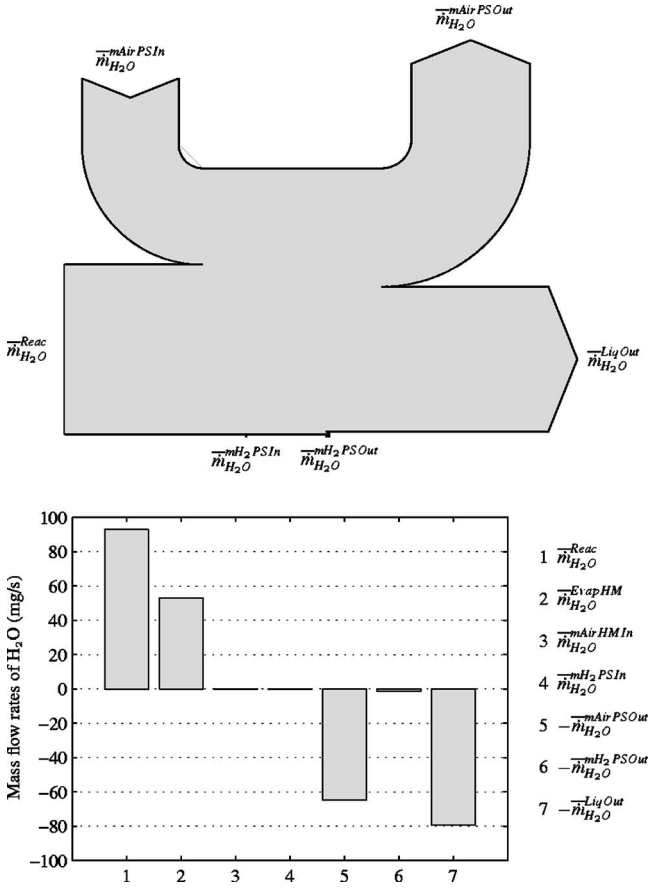

Fig. 7 Averaged contributions to the (steady-state) water mass balance for the gas channels

this experiment, about 86% of the product water exits the system in liquid form ($\dot{m}_{H_2O}^{Liq\ Out}$), the remaining 14% is evaporated. The mass of the water carried by the air is much larger than that carried by the hydrogen, despite the higher storage capacity of water mass per unit mass of hydrogen. This effect is mainly due to the significant difference in the mass flow rate of the excess air and the mass flow rate of the purged hydrogen ($\bar{\dot{m}}_{Air}^{Excess}$ =590 mg/s, $\bar{\dot{m}}_{H_2}^{Purge}$=1.0 mg/s). About 53 mg of coolant are evaporated per second inside the humidification section ($\dot{m}_{H_2O}^{Evap\ HM}$), which is 0.35% of the total coolant mass flow rate of approximately 15.3 g/s.

Sensitivity Analysis. The equations of the energy balance contain physical constants, material properties, system parameters, measurement data values, and estimated signals. However, the measured signals are subject to sensor miscalibration and the system parameters as well as the four estimated signals are subject to modeling errors. In order to quantify the influence of uncertainty in these variables, a first-order sensitivity analysis was performed. Following Eq. (31), the underlying equation of the sensitivity analysis was defined as

$$\frac{dU}{dt} + \Delta\left(\frac{dU}{dt}\right)_j = f(\xi_j + \Delta\xi_j) \tag{34}$$

where

$$\frac{dU}{dt} = f(\xi), \quad \xi: \text{ parameters, signals} \tag{35}$$

In the sensitivity analysis the impact $\Delta(dU/dt)_j$ of signal offsets or of parameter deviations, $\Delta\xi_j$, from their nominal values, ξ_j, on the rate of change in internal energy of the system, dU/dt, is investigated (one-at-a-time experiments). The nominal conditions were set to the average values of the experiment shown in Fig. 3 and to the estimated values stated in the energy balance section. This corresponds to typical operating conditions with an electric output power of approximately 730 W. The offsets and deviations, $\Delta\xi_j$, were chosen to reflect the uncertainty of the corresponding quantity, which is the calibration and sensor tolerance for the measurement signals and a judicious guess of the uncertainty for the estimated signals and the system parameters.

Table 2 Results of the sensitivity analysis

Quantity	Nom. value ξ_j	Deviation $\Delta\xi_j$	Sensitivities S_j (W)	Sensitivities s_j (%)
$T_{Ct}^{PS\ In}$	46°C	1°C	64	8.7
$\dot{m}_{Ct}^{PS\ In}$	920 g/min	20 g/min	−8.4	−1.1
$T_{mAir}^{HM\ In}$	20°C	5°C	3.4	0.46
$\dot{m}_{H_2O}^{mAirHM\ In}$	0 mg/s	1.2 mg/s	2.8	0.38
$p_{mH_2}^{PS\ Out}$	1.013 bar	0.05 bar	0.18	0.025
$\dot{m}_{H_2}^{Leak}$	0.56 mg/s	0.28 mg/s	0.92	0.13
α_{B2Amb}	3.9 W/(m^2 K)	1 W/(m^2 K)	−12	−1.7
ε	0.9	0.1	−8.4	−1.1

Table 2 shows the results of the sensitivity analysis for a selection of sensor signals with high sensitivities, for the estimated signals, and for two system parameters. The sensitivities are listed as absolute values, S_j, and as fractions, s_j, of the waste heat of the electrochemical reaction,

$$S_j = \Delta\left(\frac{dU}{dt}\right)_j$$
$$s_j = \frac{S_j}{\bar{\dot{H}}_{Reac} - \bar{P}_{El}} \tag{36}$$

From all sensor signals, the one with the highest impact on the energy balance is the temperature of the coolant at the power section inlet, $T_{Ct}^{PS\ In}$. A sensor or calibration error of 1 K results in an error of 64 W in the energy balance. This error merits special attention since it corresponds to 8.7% of the total waste heat of the electrochemical reaction. An assumed error of 20 g/min in the coolant mass flow measurement leads to an offset of −8.4 W in the energy balance. The sensitivities of the estimated signals $T_{mAir}^{HM\ In}$, $\dot{m}_{H_2O}^{mAir\ HM\ In}$, $p_{mH_2}^{PS\ Out}$, and $\dot{m}_{H_2}^{Leak}$ reveal that the uncertainty in these quantities does not much affect the energy balance. For the temperature a deviation of 5 K was chosen and the deviation of the mass of vapor in the (dried) inlet air stream was chosen to be 2% of the vapor mass in the outlet air stream. The deviation of the anode outlet pressure was set to 5000 Pa, which is about 5% of the nominal value, and the deviation of the leakage mass flow rate was set to 50% of its nominal value. The impacts on the energy balance are 3.4 W, 2.8 W, 0.18 W, and 0.92 W, respectively. A change of 1 W/(m^2 K) in the heat transfer coefficient, α_{B2Amb}, results in an offset of −12 W in the energy balance, whereas an uncertainty of 0.1 in the emissivity, ε, corresponds to an offset of −8.4 W.

The results of the sensitivity analysis demonstrate that accurate temperature sensors and good sensor calibration are of paramount importance for the parametrization of low-temperature systems such as PEM fuel cell systems. As the evaluation of the sensitivity of the coolant inlet temperature measurement and the evaluation of the sensitivity of the heat transfer coefficient do not mutually

interact, i.e., each sensitivity is independent of the other parameter's nominal value, the results listed in Table 2 allow the conclusion that an error of just 1 K in the coolant inlet measurement would lead to an approximate error of 5 $W/(m^2 K)$ in the convective heat transfer coefficient. This result is alarming, as the 5 $W/(m^2 K)$ are 130% of the coefficient's nominal value. It is noteworthy that the authors in [1] document a significant disagreement between the convective heat transfer coefficient derived experimentally and the values expected from standard natural convection. The sensitivity analysis can help to determine the required accuracy of every sensor, if Eq. (34) is evaluated from left to right. Starting with a tolerated uncertainty, $\Delta(dU/dt)$, the sensor tolerances, $\Delta\xi_j$, can be calculated.

Control-Oriented Model

A model has to capture the system's main static and dynamic phenomena without creating an excessive computational burden in order to be usable for control purposes (e.g., temperature controller designs, warm-up optimizations). In the following, a lumped-parameter approach based on physical first principles is applied. The spatial inhomogeneities in the stack temperature and in the heat transfer coefficients are ignored. Complex phenomena such as membrane humidification or water transport perpendicular to the membrane are not considered either, as they are deemed to be irrelevant within the scope of this model.

As a first step in the development of a control-oriented model, the system boundaries have to be set up, i.e., its input and output signals have to be defined. Then, all relevant dynamic phenomena of the system have to be identified. These are the dynamics that exhibit transients similar to the system output transients. Fast dynamics can be modeled statically and slow dynamics as constants. For the thermal model of the fuel cell system the variable of main interest is the bulk system temperature. The time constant associated with the bulk temperature dynamic can be estimated by analyzing Eq. (1). Depending on the operating conditions a time constant of about 10^2 s is calculated. The time constants of the electrochemistry, of the RC element of the electrode/membrane system, and of the hydrogen and air manifold dynamics are several orders of magnitude faster. In [6] these time constants are estimated to be in the order of magnitude of 10^{-9} s for the electrochemistry and the RC element and of 10^{-1} s for the manifold dynamics, respectively. As a consequence, these dynamics may be modeled as quasistatic processes when thermal management is considered. Rough calculations for the thermal dynamics of the coolant mass inside the power section and the coolant mass inside the humidifier reveal time constants of about 10 s.

Based on this analysis the fuel cell system was modeled to consist of three dynamic subsystems: the body of the fuel cell system, the coolant inside the power section, and the coolant inside the humidifier. The corresponding state variables are the bulk fuel cell system temperature, T_B, the mean temperature of the coolant mass inside the power section, T_{Ct}^{PS}, and the mean temperature of the coolant mass inside the humidification section, T_{Ct}^{HM}. All other dynamics are considered to be fast and thus are modeled quasistatically. A schematic overview of the subsystems is given in Fig. 8. In order to find the governing differential equations of the system dynamics a control volume approach is applied to each subsystem. Thus, the energy balance of Eq. (1) splits into three differential equations, i.e., one for each subsystem. These equations are coupled through energy flows interacting among the subsystems. A causality and input-output diagram of the fuel cell system model is depicted in Fig. 9. Based on the current demand, I_{St}, and the coolant inlet conditions, $T_{Ct}^{PS\ In}$ and $\dot{m}_{Ct}^{PS\ In}$, the model predicts the system temperature, T_B, the coolant outlet temperature, $T_{Ct}^{HM\ Out}$, and the stack voltage, V_{St}. Hence, the model exhibits its three input and three output signals.

In the following, the differential equations of the subsystems are stated and all the energy flows crossing the boundaries and

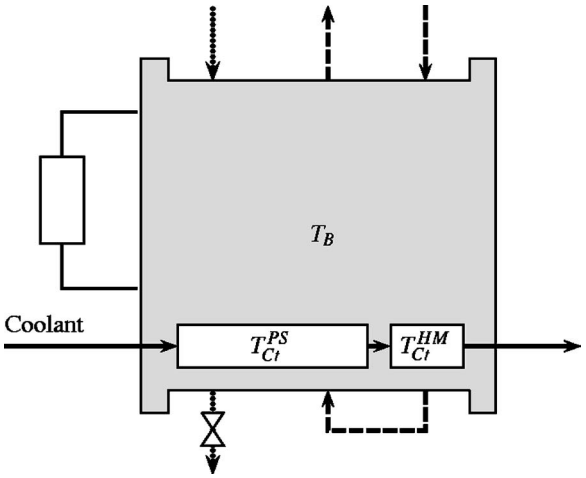

Fig. 8 Dynamic subsystems of the fuel cell system model with the state variables T_B, T_{Ct}^{PS}, and T_{Ct}^{HM}

those interacting among the subsystems are modeled. For two reasons this modeling effort is more extensive than the energy balance analysis presented in the previous section. First, there are three control volumes that correspond to three dynamical states instead of one. Second, many internal signals have to be modeled as well. The errors associated with modeling the intermediate signals propagate and can potentially increase the model error. However, the results from the previous section can be utilized to define the relevant contributions to the thermal dynamics and allow the simplification of the control-oriented model.

Body and Gas Channels. Applying a control volume analysis to the fuel cell system body yields the following energy balance differential equation:

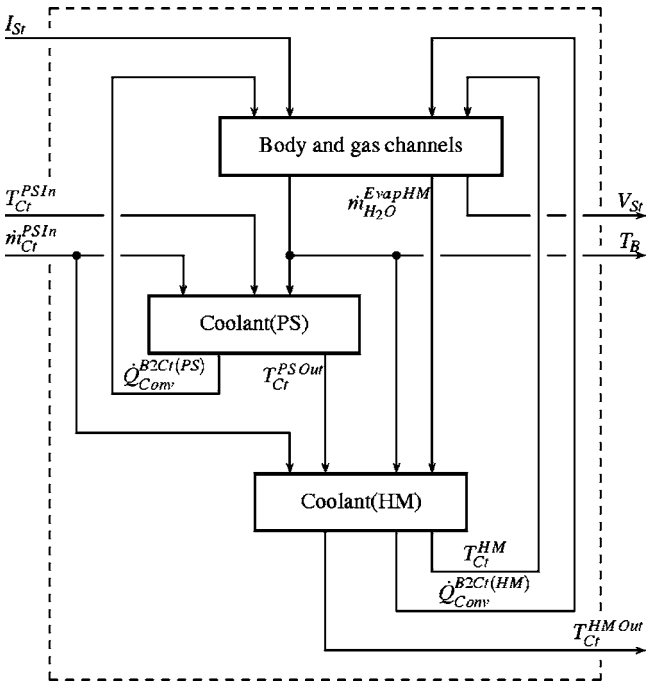

Fig. 9 Causality diagram of the dynamic fuel cell system lumped-parameter model with the input signals I_{St}, $T_{Ct}^{PS\ In}$, $\dot{m}_{Ct}^{PS\ In}$ and the output signals V_{St}, T_B, $T_{Ct}^{HM\ Out}$

$$m_B C_B \frac{dT_B}{dt} = \dot{H}_{Reac} - \dot{H}_{H_2O}^{Evap\ PS} + \Delta\dot{H}_{mAir}^{Excess} - \dot{Q}_{Conv}^{B2Ct(PS)} - \dot{Q}_{Conv}^{B2Ct(HM)} - \dot{Q}_{Conv}^{B2Amb} - \dot{Q}_{Rad}^{B2Amb} - P_{El} \quad (37)$$

Below, this equation is explained and also compared with the energy balance of the entire system (Eq. (1)). As the thermal capacity of the fuel cell system body, $m_B C_B$, differs from the thermal capacity of the total system, the index B is introduced here. The reaction enthalpy flow, $\dot{H}_{Reac}$, is calculated according to Eq. (2). In order to calculate the enthalpy difference of the reactants and the product from the present state to the reference state, the respective inlet and outlet temperatures have to be modeled. A water mass balance has to be implemented to calculate the enthalpy flow of evaporation inside the power section, $\dot{H}_{H_2O}^{Evap\ PS}$. The mass flow rate of the evaporated product water is calculated as the difference between the inflowing and the effused mass flow rates of vapor. The water contents of the air stream at the power section inlet and the power section outlet are determined from modelled temperature, pressure, and relative humidity values. The vapor on the anode side is neglected, as the mass flow rates are comparably small (see Fig. 7, mass flow rates 4 and 6). The calculation of the enthalpy difference of the moist excess air, $\Delta\dot{H}_{mAir}^{Excess}$, needs the mass flow rate of dry air and the mass flow rate of vapor carried by the air at the inlet to be known. As apparent from Fig. 5 and Table 1 and as discussed earlier, the enthalpy flows of the leaking hydrogen and of the purged moist hydrogen are small compared to the other enthalpy flows and, as a consequence, may be neglected. The energy carried away by the coolant is modeled as two convective heat flows: the heat flow from the body to the coolant mass inside the power section, $\dot{Q}_{Conv}^{B2Ct(PS)}$, and the heat flow to the coolant mass inside the humidification section, $\dot{Q}_{Conv}^{B2Ct(HM)}$. The energy removed by the evaporation of coolant is accounted for in the humidifier coolant mass subsystem. The remaining terms of Eq. (37) coincide with the corresponding terms of Eq. (1).

In order to predict the voltage output of the fuel cells, a quasistatic electrochemical model was implemented. In previous studies, for example [7–9], different voltage models have been developed. In the present study, the model of [9] was adopted. The cell voltage is written as the thermodynamic potential E minus the activation overvoltage, ν_{Act}, minus the Ohmic overvoltage, ν_{Ohm}, minus the concentration overvoltage, ν_{Conc},

$$V_{Cell} = E - \nu_{Act} - \nu_{Ohm} - \nu_{Conc} \quad (38)$$

where

$$E = E(T_B, p_{H_2}^{PS}, p_{O_2}^{PS}) \quad (39)$$

$$\upsilon_{Act} = \upsilon_{Act}(i, p_{mAir}^{PS}, T_{mAir}^{PS}, p_{O_2}^{PS}) \quad (40)$$

$$\upsilon_{Ohm} = \upsilon_{Ohm}(i, T_B, \lambda_m) \quad (41)$$

$$\upsilon_{Conc} = \upsilon_{Conc}(i, T_B, p_{O_2}^{PS}, T_{mAir}^{PS}) \quad (42)$$

The variable λ_m denotes the membrane water content, i is the current density, which equals the stack current per active area, and $p_{H_2}^{PS}$ and $p_{O_2}^{PS}$ are the partial pressures of hydrogen in the anode and oxygen in the cathode, respectively. In the present study, the membrane hydration is assumed to be constant (fully humidified membrane presumed). The partial pressures can be calculated from the total pressures, the relative humidities, and the saturation pressures on the anode and cathode sides, respectively. The overvoltages are expressed as a combination of physical and empirical relationships. The empirical parameters were determined in [9] using nonlinear regression on fuel cell polarization data. The stack voltage is defined as the sum of all individual cell voltages,

$$V_{St} = n_{Cells} V_{Cell} \quad (43)$$

A quasistatic model of the gas channels is implemented to provide data on temperature, pressure, relative humidity, and mass flow rate. The pressure drop over the cathode channel is described by a linearized nozzle,

$$p_{mAir}^{PS\ In} = p_{mAir}^{PS\ Out} + \frac{\dot{m}_{Air}^{HM\ In}}{k_p} \quad (44)$$

where the nozzle constant k_p can be determined by parameter identification. The pressure at the cathode outlet, $p_{mAir}^{PS\ Out}$, is set to ambient pressure. The mass flow rate of dry air entering the system, $\dot{m}_{Air}^{HM\ In}$, is modeled proportional to the mass flow rate of reactant oxygen,

$$\dot{m}_{Air}^{HM\ In} = \lambda_{Air} \frac{1}{0.21} \frac{M_{Air}}{M_{O_2}} \dot{m}_{O_2}^{Reac} \quad (45)$$

where the air excess ratio, λ_{Air}, is considered to be a known operating parameter that is perfectly controlled through the reactant control subsystem (typically within the range 2.0–3.5). Assuming the hydrogen supply to be perfectly controlled as well, the anode inlet pressure is modeled as a constant. The anode outlet pressure is approximated as ambient pressure. Anode and cathode pressures are determined as the mean of the respective inlet and outlet pressures. The temperatures of both gas streams are assumed to be known at the inlets. Their values are selected based on the ambient conditions, but the selection is not very critical as can be shown. Hence, they are included in the model as non-varying input parameters. The air temperature at the humidifier outlet (the power section inlet) is defined to be equal to the temperature of the coolant inside the humidification section. In order to calculate the air temperature at the power section outlet, the following approach is taken,

$$T_{mAir}^{PS\ Out} = 2 \cdot T_{mAir}^{PS} - T_{mAir}^{PS\ In} \quad (46)$$

where

$$T_{mAir}^{PS} = T_B - \frac{\dot{H}_{Reac} - P_{El}}{k_T} \quad (47)$$

Here, it is assumed that the temperature difference between the body of the fuel cell and the cathode air is proportional to the total waste heat of the reaction. The constant of proportionality is defined as $1/k_T$, which can be determined experimentally. This simple model yields satisfactory agreement with measurement data. The temperature of the hydrogen in the anode is calculated as the mean value of the hydrogen inlet and outlet temperatures, with the temperature of the hydrogen at the outlet assumed to be equal to the temperature of the system body. This assumption is justified because of the small mass flow rate. The water content of the air supplied at the humidifier inlet is directly assigned as an input parameter. At the humidifier outlet (the power section inlet, respectively), the air stream is presumed to be saturated. The relative humidity of the air stream at the power section outlet is also set to one, provided that enough water enters the system. Otherwise, it is assumed that all water has evaporated, and the relative humidity is modified accordingly. The relative humidity of the hydrogen is directly assigned. It is set to 0.5, as the hydrogen enters the system almost dry and leaves the system saturated, as the measurement data in Fig. 3 show.

Coolant Mass of Power Section. The governing differential equation for the energy balance of the coolant inside the power section is given as

$$m_{Ct(PS)} C_{Ct} \frac{dT_{Ct}^{PS}}{dt} = \Delta\dot{H}_{Ct}^{PS} + \dot{Q}_{Conv}^{B2Ct(PS)} \quad (48)$$

The time derivative of the lumped temperature is a function of the enthalpy difference of the coolant flow, $\Delta\dot{H}_{Ct}^{PS}$, and of the convective heat transfer rate, $\dot{Q}_{Conv}^{B2Ct(PS)}$. The enthalpy difference of the

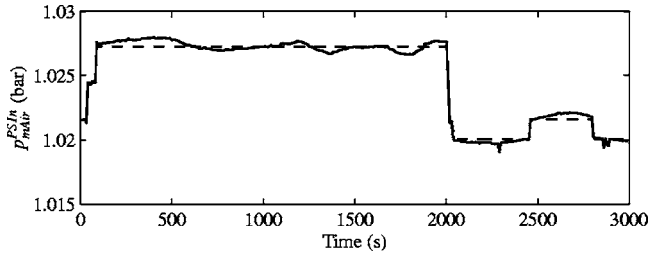

Fig. 10 Parametrization of the cathode inlet pressure model; experiment (—) and model (– – -)

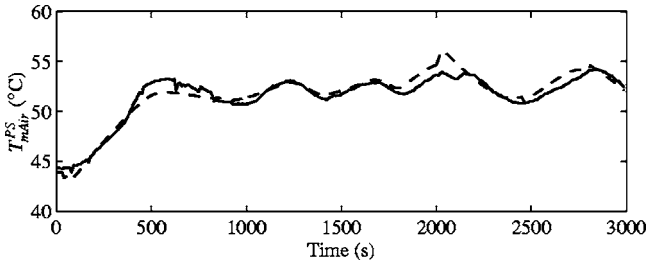

Fig. 11 Parametrization of the cathode temperature model; experiment (—) and model (– – -)

coolant flow depends on the coolant mass flow rate and on the coolant temperatures at the power section inlet and outlet. The coolant mass flow rate and the inlet temperature are input signals and thus given. At the outlet, the temperature is calculated as a function of the lumped temperature as

$$T_{\mathrm{Ct}}^{\mathrm{PS\ Out}} = 2 \cdot T_{\mathrm{Ct}}^{\mathrm{PS}} - T_{\mathrm{Ct}}^{\mathrm{PS\ In}} \tag{49}$$

The convective heat transfer rate from the body to the coolant inside the power section is modeled according to Newton's law of cooling as

$$\dot{Q}_{\mathrm{Conv}}^{\mathrm{B2Ct(PS)}} = (\alpha A)_{\mathrm{B2Ct(PS)}} \cdot (T_{\mathrm{B}} - T_{\mathrm{Ct}}^{\mathrm{PS}}) \tag{50}$$

where $A_{\mathrm{B2Ct(PS)}}$ is the heat transfer area and $\alpha_{\mathrm{B2Ct(PS)}}$ the heat transfer coefficient. The heat transfer coefficient is a function of the geometry, the medium properties, and the flow conditions. The geometry is constant, and for small temperature variations the medium properties are constant as well, whereas the flow conditions can change. In formal analogy to heat transfer correlations for forced convection, the following simple approach is used to define the heat transfer coefficient as a function of the mass flow rate of the coolant:

$$\alpha_{\mathrm{B2Ct(PS)}} = K_h \cdot (\dot{m}_{\mathrm{Ct}}^{\mathrm{PS}})^{\delta_h} \tag{51}$$

The coefficients K_h and δ_h are determined experimentally.

Coolant Mass of Humidification Section. The energy balance of the coolant inside the humidification section is similar to the energy balance of the power section coolant mass (Eq. (48)),

$$m_{\mathrm{Ct(HM)}} C_{\mathrm{Ct}} \frac{dT_{\mathrm{Ct}}^{\mathrm{HM}}}{dt} = \Delta \dot{H}_{\mathrm{Ct}}^{\mathrm{HM}} - \dot{H}_{\mathrm{H_2O}}^{\mathrm{Evap\ HM}} + \dot{Q}_{\mathrm{Conv}}^{\mathrm{B2Ct(HM)}} \tag{52}$$

but it also comprises an enthalpy flow of evaporation, as one part of the coolant is evaporated to humidify the air stream. The coolant temperature at the humidifier outlet is calculated as a function of the lumped temperature as

$$T_{\mathrm{Ct}}^{\mathrm{HM\ Out}} = 2 \cdot T_{\mathrm{Ct}}^{\mathrm{HM}} - T_{\mathrm{Ct}}^{\mathrm{PS\ Out}} \tag{53}$$

The convective heat flow term is modeled analogously to Eq. (50) as

$$\dot{Q}_{\mathrm{Conv}}^{\mathrm{B2Ct(HM)}} = (\alpha A)_{\mathrm{B2Ct(HM)}} \cdot (T_{\mathrm{B}} - T_{\mathrm{Ct}}^{\mathrm{HM}}) \tag{54}$$

where the heat transfer coefficient of the humidification section is assumed to be equal to the heat transfer coefficient of the power section,

$$\alpha_{\mathrm{B2Ct(HM)}} = \alpha_{\mathrm{B2Ct(PS)}} = \alpha_{\mathrm{B2Ct}} \tag{55}$$

Parameter Identification. Four parameters were determined experimentally using the measurement data shown in Fig. 3. The nozzle constant of the cathode, k_p, can be determined by substituting data of the cathode inlet pressure, the cathode outlet pressure, and the air mass flow rate into Eq. (44). A comparison of experiment and model (Eq. (44)) is shown in Fig. 10 using the nozzle constant identified.

The cathode temperature parameter, k_T, was determined by matching the predicted cathode temperature with the experimental cathode temperature, where the latter was defined as the mean of the measured air temperatures at the power section inlet and the power section outlet. Figure 11 shows the validation of the model (Eq. (47)) using the cathode temperature parameter identified.

In order to determine the heat transfer coefficient from the block to the coolant, α_{B2Ct}, for different mass flow rates, the experimental data was split into three sections. For these three sections, each with approximately constant coolant mass flow rate (see Fig. 3, subplot 2), the heat transfer coefficient was varied to match the simulated with the measured coolant outlet temperature. The resulting values are shown in Fig. 12, represented by small squares. In a subsequent step, the parameters K_h and δ_h were determined by curve fitting (Fig. 12, continuous line). For this parameter identification, at least the following data are required: the stack current, the coolant mass flow rate, the coolant inlet, and outlet temperatures, the cathode inlet and outlet temperatures. The accuracy of the resulting values can be improved by using experimental data for the stack voltage, the air mass flow rate, and the cathode inlet pressure and relative humidity as well.

In Table 3 all parameters of the fuel cell system model are summarized, except for the coefficients of the voltage equation which can be found in [9]. At the bottom of the table the values of the four experimentally determined parameters are specified. Most of the other parameters are geometrical parameters and are thus determined in a straightforward fashion. The specific heat of the fuel cell system body, C_{B}, was calculated as the mass-weighted sum of the specific heats of the system components. The convective heat transfer coefficient, $\alpha_{B2\mathrm{Amb}}$, was calculated and the emissivity, ε, was estimated as discussed in the energy balance section.

Validation Results. The model parameters were identified based on the experimental data presented in Fig. 3. In order to show that the model can emulate the system behavior it has to be validated with a set of experimental data different from the data used for parameter identification. Therefore, the coolant outlet temperature was compared with the corresponding measurement data of two additional experimental runs. During these experiments the model input signals (electric current, coolant mass flow rate, and coolant inlet temperature) were varied. By changing the power level and varying the coolant inlet conditions, the system

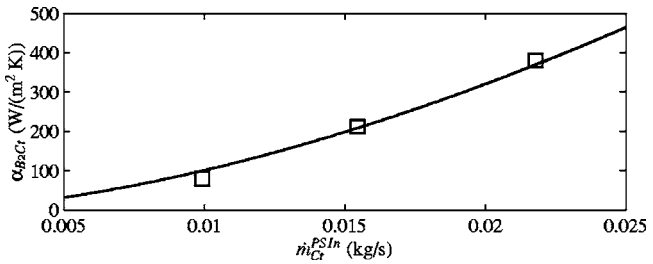

Fig. 12 Parametrization of the heat transfer coefficient model; identification data (□) and model (—)

Table 3 Parameters of the fuel cell system model (exclusive of the coefficients of the voltage equation)

Parameter	Value	Remark
n_{Cells}	24	
m_B	18 kg	
C_B	1300 J/(Kg K)	Calculated
$A_{B2\text{Amb}}$	0.44 m^2	
$\alpha_{B2\text{Amb}}$	3.9 $W/(m^2\,K)$	Calculated
ε	0.9	Estimated
A_{Active}	296×10^{-4} m^2	
λ_{Air}	2	
λ_m	14	
$m_{\text{Ct(PS)}}$	0.51 kg	
$m_{\text{Ct(HM)}}$	0.31 kg	
$A_{\text{B2Ct(PS)}}$	0.75 m^2	
$A_{\text{B2Ct(HM)}}$	0.5 m^2	
k_p	5.7×10^{-7} m s	Identified
k_T	340 W/K	Identified
K_h	2.16×10^5 $W/(m^2\,K)\cdot(kg/s)^{-1.67}$	Identified
δ_h	1.67	Identified

dynamical states are excited. The four constant input parameters of the model were set to average experimental values,

- $T_{\text{Amb}}=25\,^\circ\text{C}$
- $T_{\text{mAir}}^{\text{HM In}}=20\,^\circ\text{C}$
- $T_{\text{mH}_2}^{\text{PS In}}=40\,^\circ\text{C}$
- $\dot{m}_{\text{H}_2\text{O}}^{\text{mAir HM In}}=0$ mg/s.

In Fig. 13 the results of the model validation are shown. Despite its simple structure, for both measurement data sets, the model reproduces the behavior of the system accurately. During the first experiment the maximum prediction error is 1.4 K, whereas for the second experiment the maximum error is 2.3 K. The good agreement of the measured and the predicted temperature curves, even during heavy transients, reveals that the model derived captures the main static and dynamic properties of the system as expected.

Discussion and Conclusions

A control volume analysis and a sensitivity analysis have been performed for the PEM fuel cell system with integrated humidification section. The first-law analysis and the water mass balance for the gas channels provided insights into the complex phenomena affecting the thermal dynamics. These findings were then used to distinguish between relevant and negligible contributions to the thermal dynamics of the system (reduction of system complexity). In particular, the results showed that the enthalpy flow of the leaking hydrogen, the enthalpy flow of the purged moist hydrogen, and the mass flow of vapor on the anode side have minor influence and are thus negligible. The sensitivity analysis revealed the importance of the sensor calibration for the experimental parameter identification.

Based on the preliminary investigations a control-oriented dynamic model of the fuel cell system was developed. This mathematical model represents a concise description of the system (as simple as possible and as accurate as necessary), which predicts the bulk fuel cell transient temperature and voltage as a function of only three input signals, namely the current drawn, the coolant inlet temperature, and the coolant mass flow rate. Unlike other existing thermal models, it includes the gas supply system. The gas conditions thus do not appear as system inputs and therefore do not have to be provided through cumbersome measurements or another simulation model. Despite its simplicity, the predictions obtained with this model match the experimental data well, as shown in the validation section. Dynamic as well as static phenomena are reproduced accurately. The physically motivated synthesis yields a model which is adaptable to different PEM fuel cell systems with little effort, as there are only a few experiments necessary for parameter identification. With some adaptations, the model should moreover be transformable to systems without an internal humidification section. The lumped-parameter approach produced a system which mathematically can be described by a

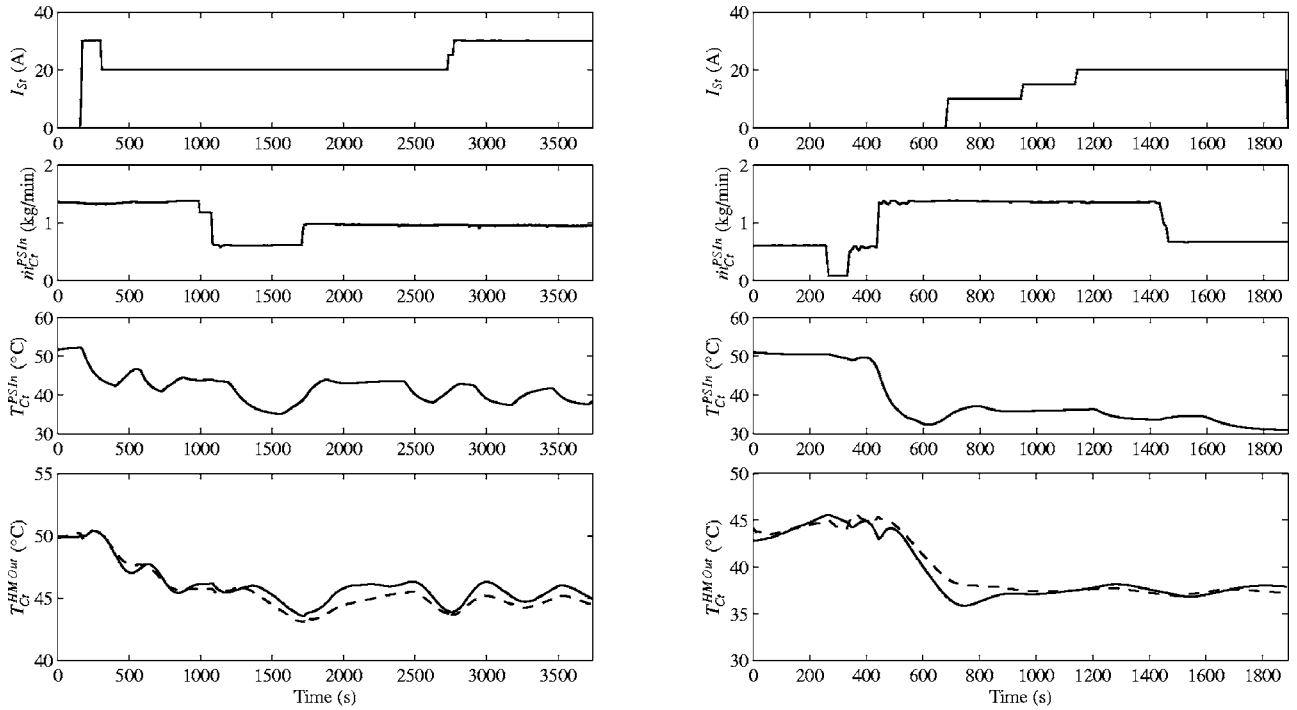

Fig. 13 Validation of the model; in each plot, subplots 1–3 show the input signals and subplot 4 the comparison between measurement (—) and prediction (– – -) of the coolant outlet temperature

set of ordinary differential equations (time-invariant, nonlinear dynamic system of third order). Thus, the model should be readily employable for model-based thermal controller synthesis or for numerical optimizations and simulations.

Nomenclature

A = area, m^2
A_{Active} = active area, m^2
C, C_p, C_{p0} = specific heat, J/(kg K)
E = thermodynamic potential, V
F = Faraday constant, C/mol
$\dot{H}$ = enthalpy flow rate, W
h = mass specific enthalpy, J/kg
h_f^0 = mass specific enthalpy of formation, J/kg
h_{fg} = mass specific evaporation enthalpy, J/kg
I = electric current, A
i = electric current density, $\mathrm{A/m^2}$
j = index
K_h = parameter of the heat transfer coeff. model
k_p = nozzle constant of cathode channel, m s
k_T = cathode temperature parameter, W/K
M = molecular weight, kg/mol
m = mass, kg
$\dot{m}$ = mass flow rate, kg/s
n_{Cells} = number of fuel cells
P = power, W
p = pressure, Pa
p_{Sat} = saturation pressure, Pa
$\dot{Q}$ = heat flow rate, W
S = sensitivity, W
s = normalized sensitivity
T = temperature, K
t = time, s
U = internal energy, J
V = voltage, V

Greek Symbols

α = convective heat transfer coefficient, $\mathrm{W/(m^2\,K)}$
δ_h = parameter of the heat transfer coefficient model
ε = emissivity
λ_{Air} = air excess ratio
λ_m = membrane water content
ν = overvoltage, V
ξ = parameter or signal value
σ = Stefan-Boltzmann constant, $\mathrm{W/(m^2\,K^4)}$
φ = relative humidity

Subscripts and Superscripts

Act = activation
Amb = ambient
B = fuel cell system body
Cell = fuel cell
Conc = concentration
Conv = convection
Ct = coolant
El = electric
Evap = evaporation
Excess = nonreacting part of moist air flow
Gases = air, hydrogen, water vapor
g = gaseous
H_2 = hydrogen
H_2O = water
HM = humidification section
In = inlet
Leak = hydrogen flow lost through leakage
Liq, l = liquid
mAir = moist air
mH_2 = moist hydrogen
nonReac = nonreacting part of the gas flows
O_2 = oxygen
Ohm = ohmic
Out = outlet
PS = power section
Purge = moist hydrogen flow purged
Rad = radiation
Reac = reaction
St = stack
Syst = fuel cell system

References

[1] Amphlett, J. C., Mann, R. F., Peppley, B. A., Roberge, P. R., and Rodrigues, A., 1996, "A Model Predicting Transient Responses of Proton Exchange Membrane Fuel Cells," J. Power Sources, **61**(1–2), pp. 183–188.
[2] Lee, J. H., and Lalk, T. R., 1998, "Modeling Fuel Cell Stack Systems," J. Power Sources, **73**(2), pp. 229–241.
[3] Xue, X., Tang, J., Smirnova, A., England, R., and Sammes, N., 2004, "System Level Lumped-Parameter Dynamic Modeling of PEM Fuel Cell," J. Power Sources, **133**(2), pp. 188–204.
[4] Zhang, Y. J., Ouyang, M. G., Lu, Q. C., Luo, J. X., and Li, X. H., 2004, "A Model Predicting Performance of Proton Exchange Membrane Fuel Cell Stack Thermal Systems," Appl. Therm. Eng., **24**(4), pp. 501–513.
[5] Hrsg.: Verein Deutscher Ingenieure, 2002, *VDI-Wärmeatlas: Berechnungsblätter für den Wärmeübergang*, Springer, Berlin.
[6] Guzzella, L., 1999, "Control Oriented Modelling of Fuel-Cell Based Vehicles," Presentation at the NSF Workshop on the Integration of Modeling and Control for Automotive Systems.
[7] Amphlett, J. C., Baumert, R. M., Mann, R. F., Peppley, B. A., Roberge, P. R., and Rodrigues, A., 1994, "Parametric Modelling of the Performance of a 5-kW Proton-Exchange Membrane Fuel Cell Stack," J. Power Sources, **49**(1–3), pp. 349–356.
[8] Kim, J., Lee, S. M., Srinivasan, S., and Chamberlin, C. E., 1995, "Modeling of Proton Exchange Membrane Fuel Cell Performance with an Empirical Equation," J. Electrochem. Soc., **142**(8), pp. 2670–2674.
[9] Pukrushpan, J. T., Stefanopoulou, A. G., and Peng, H., 2004, *Control of Fuel Cell Power Systems: Principles, Modeling, Analysis, and Feedback Design*, Springer, London, Chap. 3.1.